Supporting Information

Solar cell fabrication

First, the perovskite solution is prepared inside a N_2-filled glovebox (water and oxygen contents less than 1 ppm) by mixing powders of PbI_2 (TCI, 99.99 %), $PbBr_2$ (TCI, 98 %), FAI (Greatcell Solar) and CsBr (Abcr, 99.999%) in molarities of (1.14 ± 0.02) M, (0.216 ± 0.004) M, (1.08 ± 0.02) M and (0.216 ± 0.005) M, respectively. All powders are introduced in the same vial before adding the solvent (4:1 DMF:DMSO). Typically 1.8 mL of solution is made for a batch of 16 samples. The solution is then heated to 75 °C until all powders are dissolved. The solution is prepared one day before the perovskite is deposited and is always stored in a sealed vial inside the N_2-glovebox.

Device fabrication starts by cleaning the 2.5x2.5 cm^2 indium tin oxide (ITO)/glass substrates (Kintec, sheet resistance of ~15 Ω/sq) using a 5 min oxygen plasma treatment followed by cleaning in an industrial glass washing machine. 20 nm of NiO is then deposited by sputtering. Before depositing the perovskite, the NiO is annealed at 300 °C for 15 min in air with a ramp of 15 min starting at room temperature. The substrates are then moved to a N_2-filled glovebox for perovskite deposition using the following two-step spin-coating recipe: 1) speed=1000 rpm, time=10s, acceleration=200 rpm/s and 2) speed=6000 rpm, time=25s, acceleration=1000 rpm/s. 100 µL of perovskite solution is used for each substrate and the solution is dropped across the entire area. Chlorobenzene is used as antisolvent, with 200 µL applied at the center of the substrate 5s before the end of the second step of the recipe. After spin-coating, the brownish samples are immediately annealed at 105 °C for 1h in a pre-heated hot plate, where they quickly become black.

Then, still inside the glovebox, 1 nm of LiF (99.98%, Sigma-Aldrich) and 19 nm of C_{60} (> 99.95%, NanoC) are thermally evaporated on top of the perovskite using a home-built system. The base pressure is 2.10^{-6} mbar or less. The rate of LiF deposition is ~0.2 A/s and that of C_{60} is ~0.5 A/s, as monitored by a quartz crystal balance.

For semitransparent devices, the samples are then taken outside of the glovebox and moved to an Oxford Instruments atomic layer deposition system where 10 nm of SnO_2 is deposited using tetrakis(dimethylamino)tin and H_2O as precursors with the substrates at 100 °C. Then, 100 nm of ITO (sheet resistance of ~80 Ω/sq) is sputtered using an Evatec cluster tool. Finally, except in cells without metal fingers, 130 nm of metal contact (Ag, Cu or a Ni/Al stack) is thermally evaporated on top of the ITO layer through a shadow mask in the form of a frame around the borders of the 0.5x0.5 cm^2 device area (see Fig. S3 for the final layout). Each substrate contains 3 devices. For opaque cells, the back metal contact is directly evaporated on top of C_{60} using a shadow mask and the back contact covers the entire area of the device.

All I-V measurements were taken using a homemade system. All semi-transparent cells are measured in superstrate configuration. The I-V curves are measured using Keithleys by increasing the applied voltage in steps and measuring the current after a determined delay. The light source is a combination of blue,

green and red LEDs and halogen lamps calibrated to 1000 W/m^2 intensity using a standard c-Si cell. The spectrum is adjusted to AM1.5G by adjusting the relative intensity of the LEDs and halogen lamps. The parameters used to make the IV curves are:

Voltage range: -0.1 V to 1.2 V in steps of 10 mV.
Delay in each step: 10 ms.
Integration time in each step: 10 ms.

For the reverse bias test protocol, after each step of reverse biasing, a forward scan (-0.1 V to 1.2 V) and then a reverse scan (1.2 V to -0.1 V) are taken. Note that fast I-V scans are acquired to capture the changes induced by the reverse bias. In the main text, all I-V curves shown are forward scans because these were taken first and therefore are more representative of the effects of the reverse bias treatments. Also, as a fast scan is used, some hysteresis is observed, as shown in Fig. S2. However, both forward and reverse curves show qualitatively similar behaviors.

Samples were prepared for transmission electron microscopy (TEM) observations using the conventional focused ion beam lift-out procedure in Zeiss NVision 40. Samples were then transferred quickly in air (<2 min) to a FEI Osiris TEM, where they were analyzed at 200 kV with scanning TEM beam current of 250 pA. Energy-dispersive X-ray spectra were quantified using the Cliff–Lorimer method implemented in the Bruker Esprit software.

Photoluminescence (PL) spectra were acquired in PL/Raman system MonoVista Confocal System using a laser with a wavelength of 514 nm.

<u>Supporting data</u>

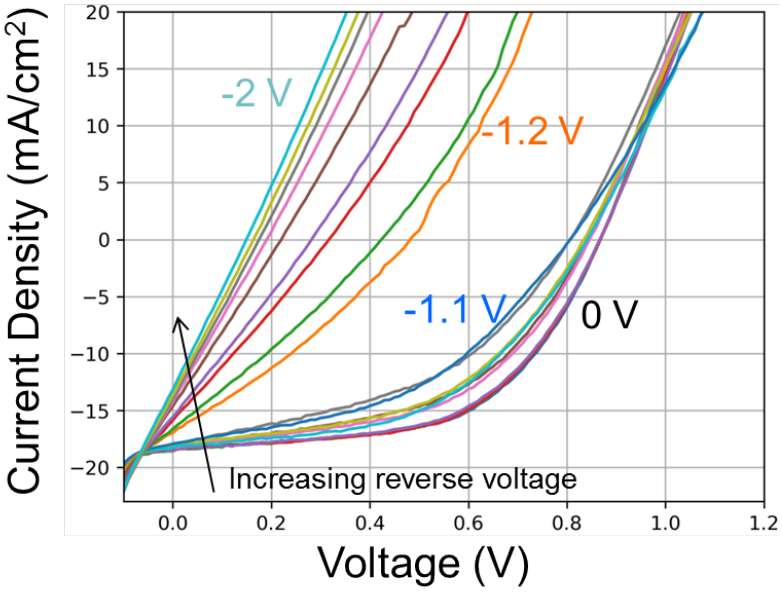

Figure S1: Typical evolution of the forward I-V scans when pre-biasing the device at progressively increasing reverse voltages. The shunt resistance decreases, while the series resistance increases.

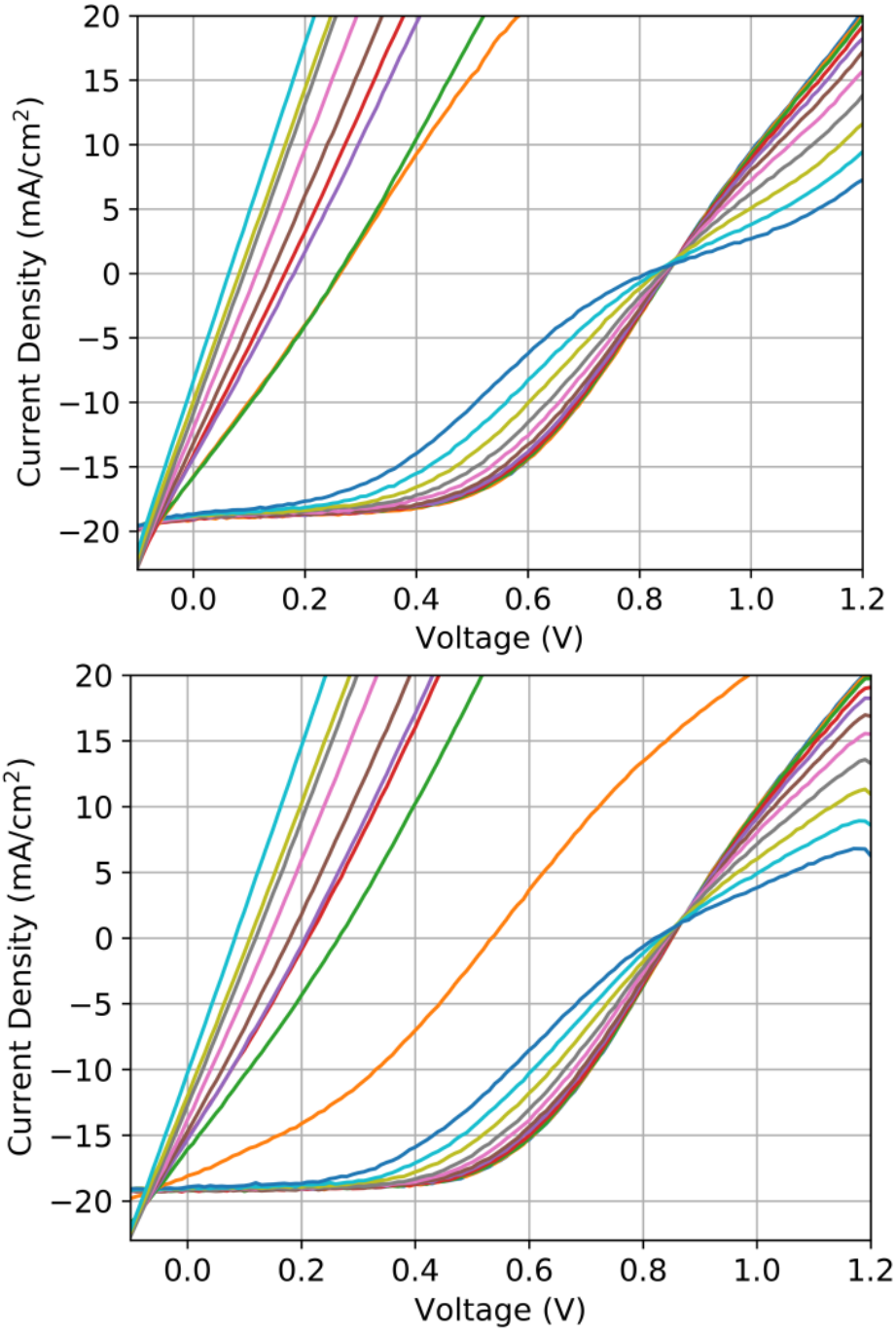

Figure S2: Forward (top figure) and reverse (bottom figure) scans taken after each reverse biasing step. Although hysteresis is present, both scans show qualitatively similar behaviors. The top figure is the same as Fig. 1b of the main text and is shown for comparison with reverse scans.

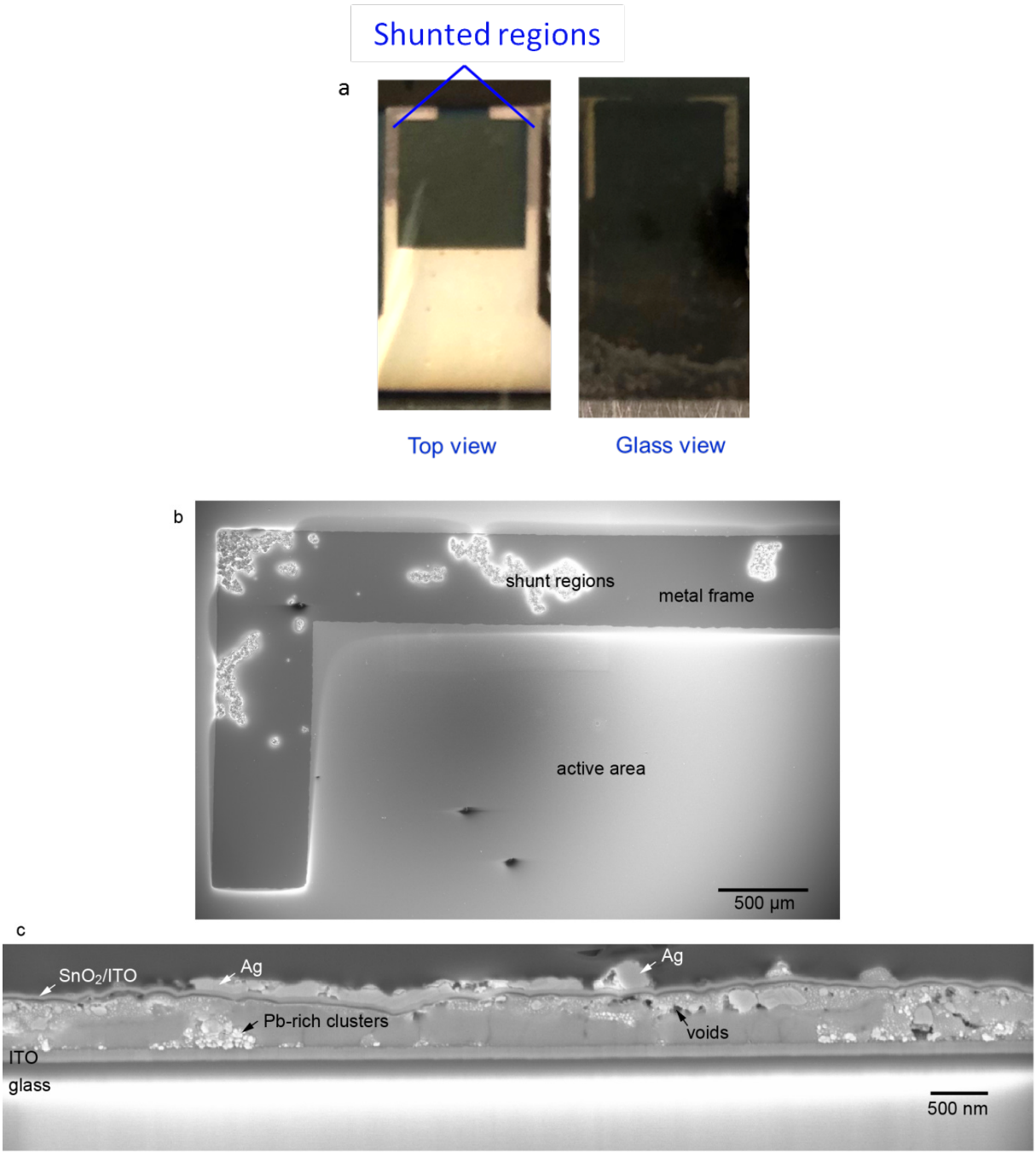

Figure S3: a) semitransparent solar cell reverse biased from 0 V to -5 V in 3 min steps of -0.1 V showing visible burn marks. The top Ag contact can be seen from the glass side. b-c) Top view and focused ion beam-prepared cross-section scanning electron microscopy images of shunted areas.

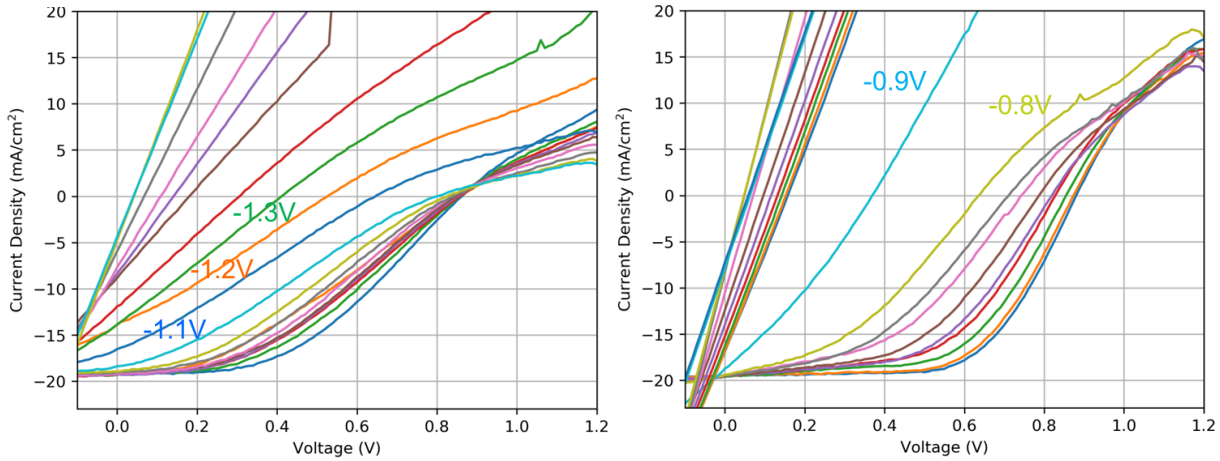

Figure S4: Evolution of the I-V curve after reverse biasing at increasing voltages for devices comprising a) Cu and b) a Ni/Al stack as back electrode.

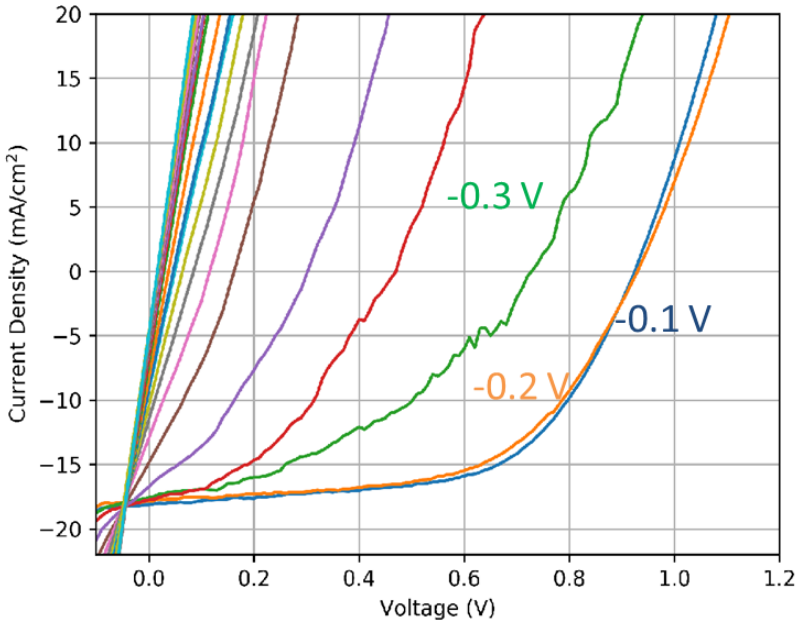

Figure S5: I-V curve evolution of an opaque solar cell, where the Ag back contact is directly on top of C_{60} and covers the entire area of the device.

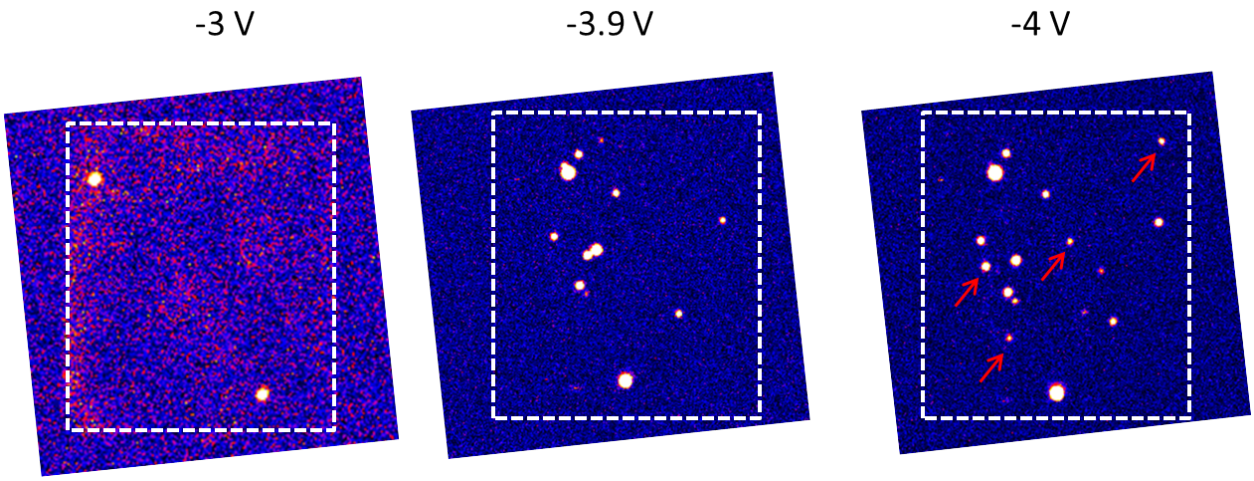

Figure S6: Hot spot formation observed with lock-in thermography in cells comprising no metallic top electrode (only ITO on top). The dashed white square delineates the region of the cell covered by the ITO electrode. At -3 V (left panel), two hot spots are observed, showing that even metal-electrode-free solar cells shunt under reverse bias, although only at heavier reverse biasing compared to cells with metal. On the middle and right panels, a comparison between images taken at -3.9 V and -4 V is shown. Arrows indicate hot spots that appeared abruptly during the -0.1 V step to -4V. The fact that these hot spots were invisible during the previous biasing step is an indication that they were created by the reverse bias itself, as opposed to simply enlarging due to heat as occurs in c-Si solar cells. These results indicate that there is also a shunting mechanism whereby the absorber layer itself degrades under reverse bias, separately to the mechanism of top metal migration.

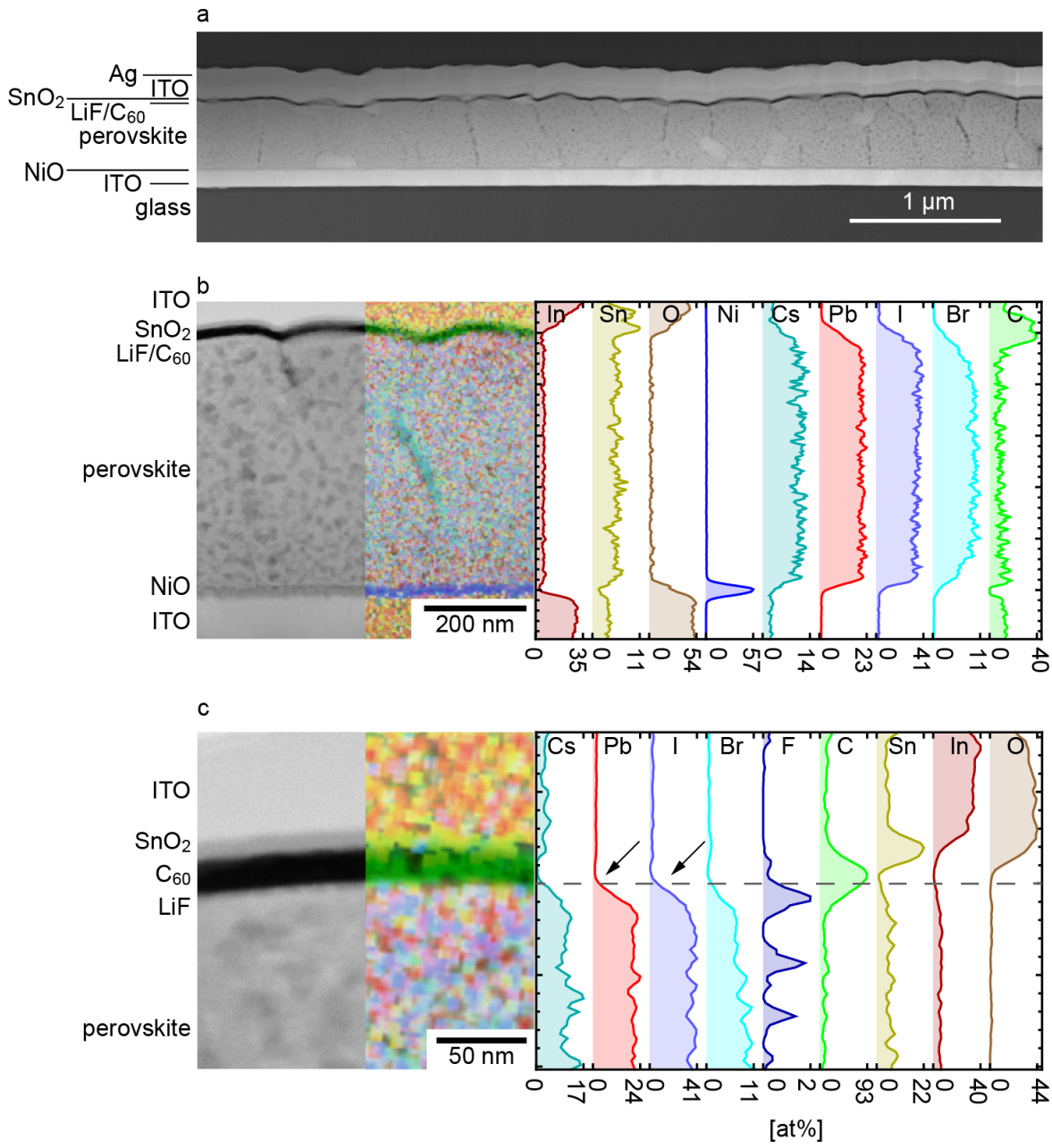

Figure S7: a) STEM HAADF image of a reference as-prepared device. The small voids are a consequence of the focused ion beam preparation of the TEM lamella. No double-layer structure is observed, contrary to Fig. 2a of the main text (sample reverse biased at -5V). (b) EDX chemical map and corresponding concentration profile of the reference sample, showing no gradient in Br (unlike Fig. 2b of the main text). (c) STEM HAADF and EDX data of the region close to the C_{60} layer. Note that the top edges of the Pb, I and Br distributions coincide in position and are well separated from the carbon peak of the C_{60} layer.

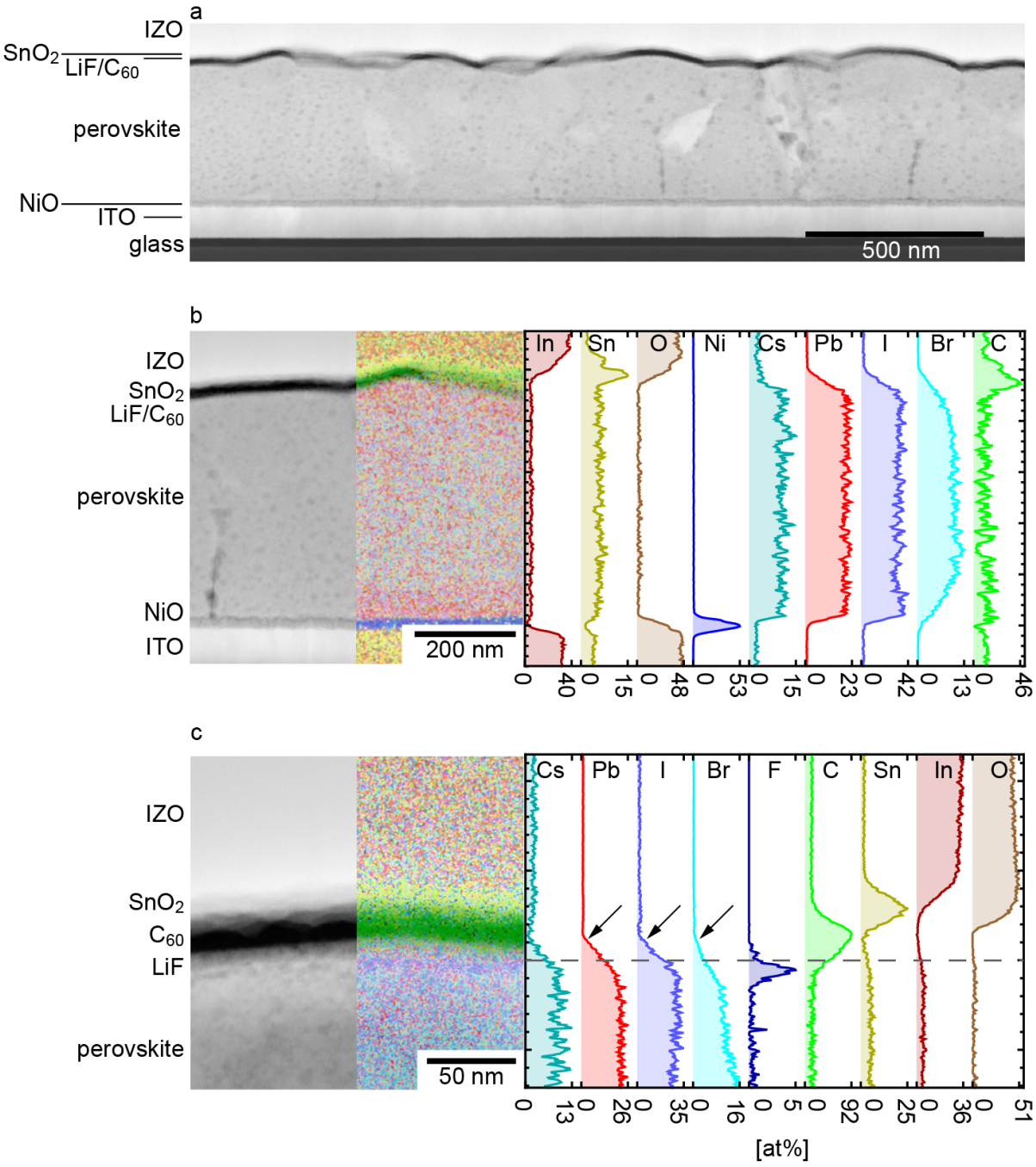

Figure S8: a) STEM HAADF image of a electrode-metal-free device after recovering from S-shape with MPPT. The small voids are a consequence of the focused ion beam preparation of the TEM lamella. (b) EDX chemical map and corresponding concentration profile of the recovered sample. (c) STEM HAADF and EDX data of the region close to the C_{60} layer. Note that the top edges of the Pb, I and Br distributions coincide in position and are well separated from the carbon peak of the C_{60} layer, corroborating our conclusion that it is the iodine inside the C_{60} layer that causes the S-shape.

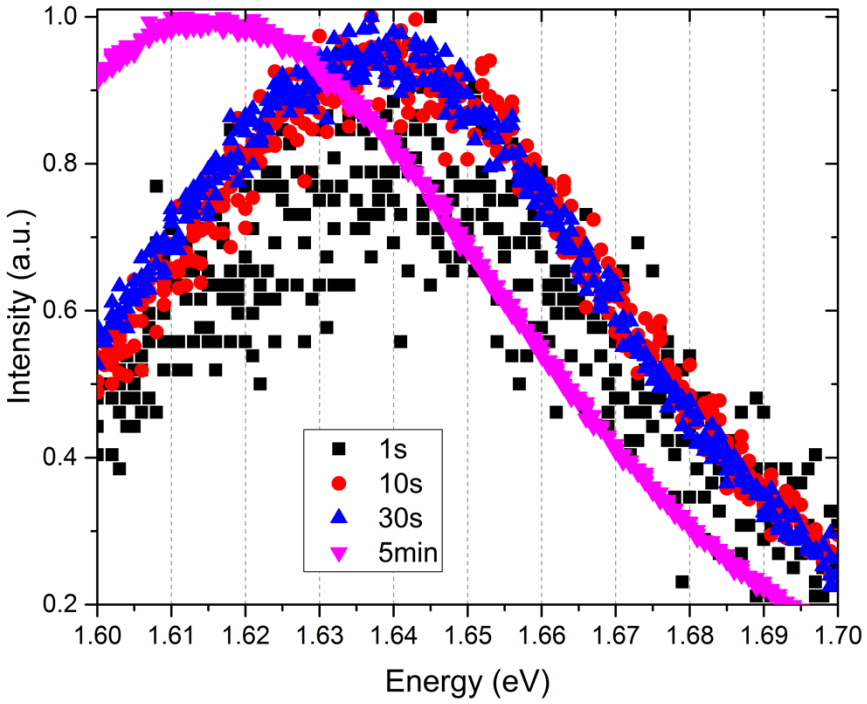

Figure S9: Normalized PL spectra measured with light intensity of 1 sun for different exposure times for a perovskite solar cell not degraded in reverse bias.

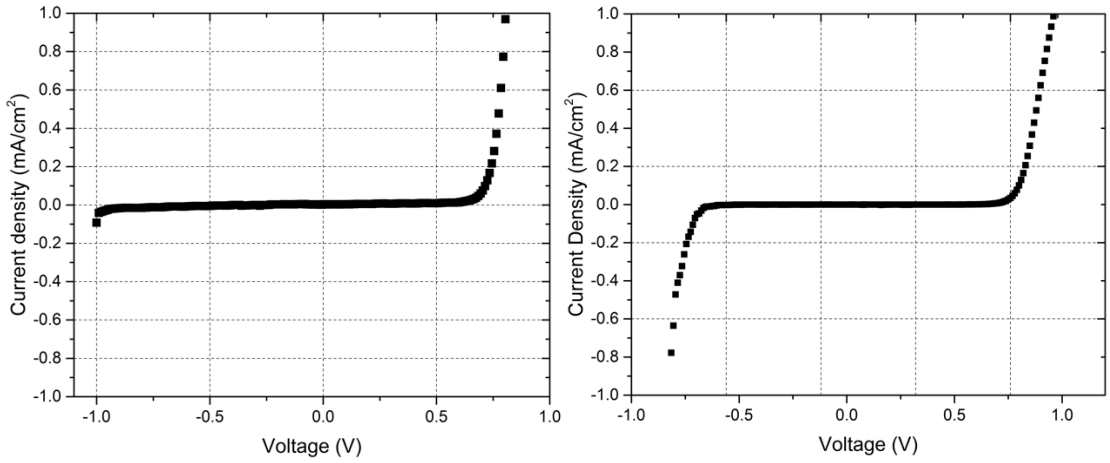

Figure S10: Dark I-V curves before degradation in reverse bias, showing the breakdown behavior. We take as definition of breakdown voltage the voltage at which the current is -1 mA/cm^2, the definition used by Bowring et al, reference 7 of the main text. The cell corresponding to the left figure was then degraded at -5 V, a voltage higher in module than the breakdown voltage, while the cell corresponding to the right figure was degraded at -0.5 V, a voltage lower than the breakdown voltage. Phase segregation was observed only for the cell degraded at a voltage higher than the breakdown voltage.

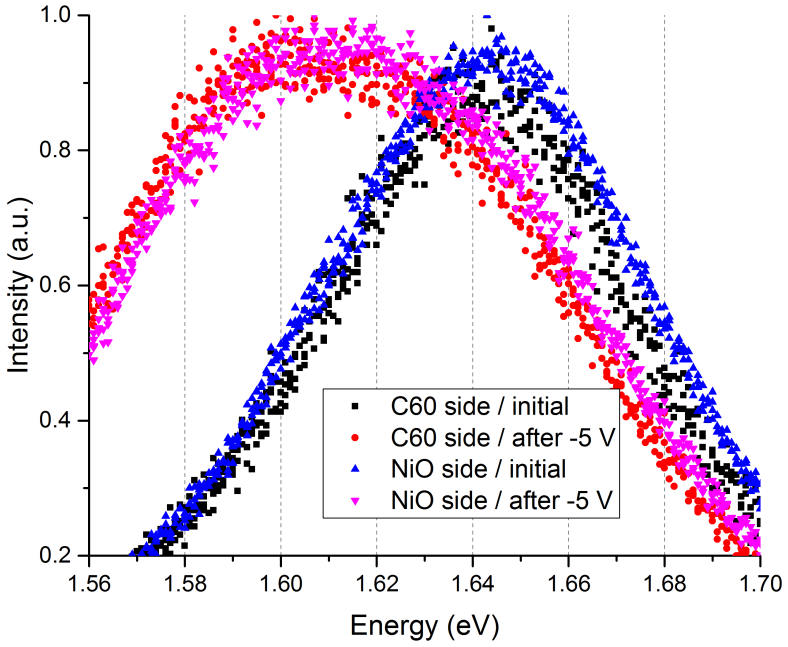

Figure S11: Normalized PL spectra of the perovskite taken from each side of a device degraded at –5 V for 30 min. A shift is observed after reverse biasing irrespective of the side from which the spectrum is acquired.

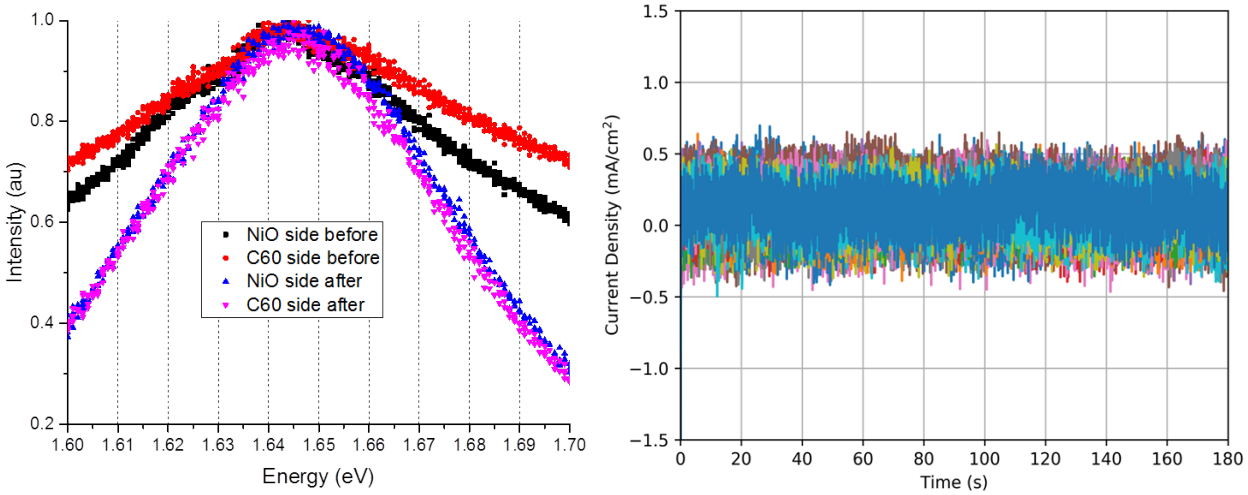

Figure S12: a) Normalized PL spectra comparing the perovskite before and after the reverse bias treatment shown in Fig. 3a of the main text. Even though the S-shape was pronounced after reverse biasing, no bandgap shift and hence no phase segregation is observed, indicating that phase segregation is not the cause of the S-shape. b) Current as a function of time during the 3 min of reverse biasing for each step of the reverse bias protocol (0 V to -2 V in steps of -0.1 V) used in this work. The negligible current injected supports the fact that no phase segregation occurred in this sample.

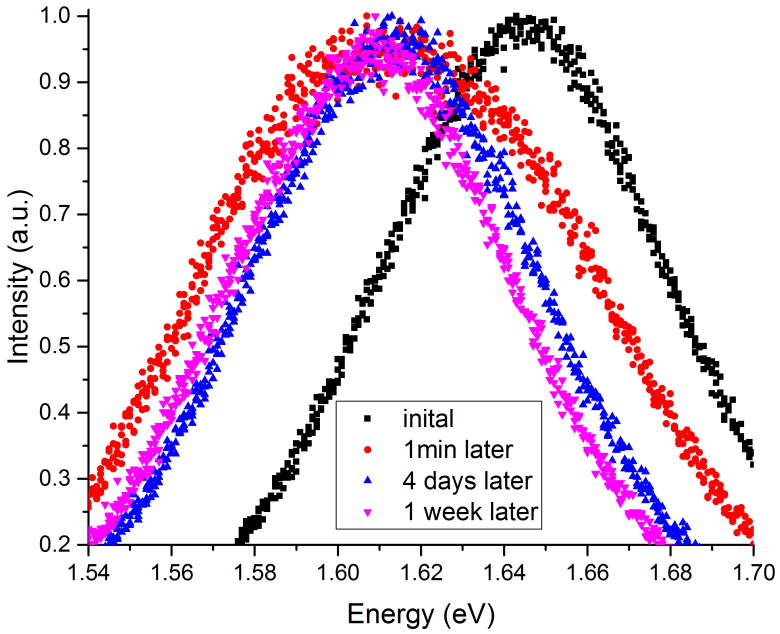

Figure S13: Normalized PL spectra measured at different times after the sample had been degraded at -5 V for 30 min, showing that the phase segregation persists even after one week after it was induced. These measurements were performed from the NiO side of the sample.